Article

Effects of Ammonium Perchlorate and CL-20 on Agglomeration Characteristics of Solid High-Energy Propellants

Xiang Lv, Rong Ma, Yuxin An, Zhimin Fan, Dongliang Gou, Peijin Liu and Wen Ao *

Science and Technology on Combustion, Internal Flow and Thermo-Structure Laboratory,
Northwestern Polytechnical University, Xi'an 710072, China
* Correspondence: aw@nwpu.edu.cn

Abstract: Energy density, which is an important indicator of the performance of solid propellants, is known to increase with the addition of 2,4,6,8,10,12-hexanitro-2,4,6,8,10,12-hexaazaisowurtzitane (CL-20). However, it remains unclear how CL-20 affects the decomposition of ammonium perchlorate (AP) and energy release. Here, the effects of CL-20 on the combustion performance and agglomeration of propellants were investigated. The addition of CL-20 decreased AP decomposition temperature and the energy required for the transformation of AP crystals from orthorhombic to cubic. The burning rate and pressure exponent of the propellant with 42% CL-20 were significantly higher than those of the propellant containing 20% CL-20. Thus, adding CL-20 to the propellant improves the energy characteristics and burning rate and the pressure exponent increases. At low combustion chamber pressure, the agglomeration of the propellant containing a high content of CL-20 will be blown away from the combustion surface only after staying on that surface for a short time. In this process, the probability of volume growth of the agglomeration after merging with other agglomerations greatly decreases, thus reducing the overall agglomerate particle sizes; further, the addition of a small amount of CL-20 to the propellant may lead to a reduction in agglomerate particle sizes. AP with a smaller particle size weakens the agglomeration in the combustion process and decreases the number of agglomerates with large particle sizes. These findings lay the foundation for the development of novel high-energy propellants.

Keywords: agglomeration; combustion; CL-20; condensed combustion products; solid propellant

1. Introduction

The energy density is the most important indicator of the performance of solid propellants. Over the past decades, solid propellants have been developed from double-base propellants to hydroxyl-terminated polybutadiene (HTPB) composite and nitrate ester plasticized polyether (NEPE) propellants. In modern composite propellants, a metal fuel (mostly aluminum powder) with a higher calorific value is one of the basic components used to increase the energy of the propellant, which can considerably enhance the energy density of the propellant. Its condensed phase combustion products (CCPs) can simultaneously inhibit high-frequency unstable combustion in solid rocket motors. However, CCPs can increase the two-phase flow loss during propellant combustion, thereby reducing the specific impulse and causing an energy loss. The factors influencing the characteristics of the ignition, combustion, and agglomeration of aluminum-based propellants have been studied extensively. The agglomeration characteristics of propellants depend on the propellant characteristics and operating environment, mainly including the size of aluminum particles [1,2], type and physical properties of metal additives [3,4], size of ammonium perchlorate (AP) particles [5,6], environment [7], type of oxidant [8–10], catalyst performance [11], and other functional additives [12–14]. Moreover, agglomerates with larger particle sizes flow at high speed in the combustion chamber and nozzle, which leads to new ablation and deposition problems [15]. The emergence and development of new high-energy density materials,

especially ammonium nitrate explosives such as 1,3,5-trinitroperhydro-1,3,5-triazine (RDX), 2,4,6,8,10,12-hexanitro-2,4,6,8,10,12-hexaazaisowurtzitane (CL-20), and octahydro-1,3,5,7-tetranitro-1,3,5,7-tetrazocine (HMX), provide practical approaches to further increase the propellant's energy level. These materials have a variety of effects on the solid propellant's combustion ability.

Ammonium nitrate-based propellants benefit from low burning temperatures, low relative molecular masses of the gas product, and low amounts of smoke, which improve the propellant energy and reduce the ablation and toxicity, but also lead to poor combustion and hinder process performance. RDX has the advantages of large power, wide source of raw materials, and good chemical stability. Liu [1] and Liu [16] et al. investigated how RDX affects the parameters of propellant combustion and agglomeration. The results showed that RDX significantly aggravates the agglomeration of Al and reduces its combustion efficiency, which may lead to the formation of a melting layer and promote the retention and agglomeration of Al particles on the combustion surface. Compared with RDX, HMX has the advantages of a high density, low impact sensitivity, and high spontaneous combustion temperature. Glotov [8] studied the effects of RDX and HMX on the agglomeration of aluminized propellants. The results showed that the combustion of RDX-based propellants leads to production of a larger amount of aluminum agglomerates, which have larger average particle sizes and higher active aluminum contents than HMX-based propellants. Compared with RDX, HMX, and other nitroamine compounds, CL-20 has a higher energy. Among the CL-20-based propellants, it has a substantially higher burning rate and pressure exponent than of HMX- and RDX-based propellants [17,18]. Zhou [19] et al. studied the effect of the CL-20 content on the combustion performance of NEPE propellants. With the increase in the CL-20 content, the burning rate, pressure exponent, and combustion efficiency of the propellant increase. Li [20] et al. studied the effects of AP, CL-20, and Al on the combustion characteristics of the propellant. The results showed that both CL-20 and AP accelerate the decomposition of NEPE propellants compared with aluminum. Wu et al. [21] studied the effects of Al and AP on CL-20 propellant agglomeration and CCPs. Their findings demonstrated that the maximum peak particle size of CCPs increases when the Al particle size decreases. An increase in the particle volume fraction of ~1 μm, increase in the degree of agglomeration, and decrease in the AP particle size led to the decrease in the maximum peak particle size of CCPs, decrease in the particle volume fraction of ~1 μm, and decrease in the degree of agglomeration. Song et al. [22] studied the effect of CL-20 on the CCPs of propellants. The results of the study showed that the replacement of HMX with CL-20 in the propellant increases the combustion efficiency of Al powder. When CL-20 completely replaces HMX in the propellant, the combustion residue rate of the propellant is the lowest. With the addition of CL-20, metastable oxides of Al, such as κ-Al_2O_3 and δ-Al_2O_3, can be observed in the CCPs of propellant combustion. The above-mentioned results indicate that compared with RDX and HMX, the combustion of propellants containing CL-20 produces fewer aluminum agglomerates and the agglomerates have smaller average particle sizes.

Although numerous studies have been conducted on the performance of solid propellants containing CL-20, these studies were not systematic, comprehensive, and thorough, and the essence of the mechanism has not been studied. Therefore, theoretical guidance regarding the performance regulation of solid propellants containing CL-20 is lacking and many uncertainties remain with respect to the performance regulation. In particular, the effects of CL-20 on the decomposition of AP and energy release remain unclear. CL-20 has a great effect on the combustion of aluminum powder. Due to the low oxidation activity of thermal decomposition products of CL-20, Al (g) reacts with CL-20 decomposition products to form metastable κ-Al_2O_3 and δ-Al_2O_3. In addition, the combustion of CL-20-based propellant is more intense, which shortens the reaction between Al (g) and the oxidant and leaves the reaction zone in advance in a manner where the agglomeration phenomenon of CCPs is weakened.

CL-20 is a compound with a high energy density and cage-shaped polycyclic nitroamine structure. In response to future developmental needs of high-efficiency solid rocket motors, the effects of CL-20 on the combustion and agglomeration of high-energy composite propellants have been analyzed in this study to address problems such as the two-phase flow loss, erosion, and combustion instability. The results of this study lay the foundation for the development of novel high-energy propellants.

2. Materials and Methods

In order to improve the specific impulse of the propellant, this study adopted measures such as adding metal powder (aluminum), energy-containing binder and replacing part of AP with high explosives in the formula, whose main components are AP, CL-20, Al, glycidyl azide polymer (GAP) and $Fe(C_5H_5)_2$, as shown in Table 1. Results of previous research showed that the particle size, content, and AP particle size of CL-20 are the main factors affecting the burning rate of the propellant. Binder type, aluminum particle size and common catalyst have no significant effect on propellant burning rate. With the increase in Al content in solid propellant, on the one hand, the energy density and burning temperature of the propellant will be significantly increased, which is beneficial to improve the specific impulse of the propellant. On the other hand, it reduces the burning rate of propellant and increases the particle size of CCP, which is not conducive to improving the specific impulse of propellant [23]. When the content of Al is about 18%, the specific impulse of composite propellant is the maximum [24]. Therefore, the variables of propellant formulation in this study are the particle size and content of AP and the content of CL-20. The contents of Al, GAP and $Fe(C_5H_5)_2$ were 18%, 27% and 1%, respectively, and remained unchanged.

Table 1. Propellant sample composition.

Propellant Number	Al		AP		CL-20	GAP	$Fe(C_5H_5)_2$
	D (μm)	wt (%)	D (μm)	wt (%)	wt (%)	wt (%)	wt (%)
C1	13	18	116	12	42	27	1
C2	13	18	69	12	42	27	1
C3	13	18	69	34	20	27	1

The experimental system for the propellant burning test is mainly composed of a combustion chamber, macro lens, high-speed camera, data acquisition system, ignition control system, and intake control system with optical observation window, as shown in Figure 1a. The propellant strand size used in the experiment was $1 \times 3 \times 25$ mm. To avoid smoke interference generated by high-pressure combustion, 1 MPa ignition condition was selected to ensure high clarity of the captured video.

CCPs of the burned propellants were collected to evaluate their physical and chemical characteristics based on the same vessel with the addition of a collection container with cooling medium (Figure 1b). The cooling medium was deionized water. The end face of the strand was 5 mm away from the liquid surface. The collected suspensions were processed by extraction and filtration, as shown in Figure 1c. Before the analysis, the products were centrifuged, washed, dried, and dispersed using ultrasonics. The microstructures of CCPs were observed with a JSM-7100F scanning electron microscope (SEM, Tokyo, Japan) produced by JEOL. The composition was detected with an X-ray Diffractometer Empyrean X-ray diffractometer (XRD, Phnom Penh, Cambodia). The Hydro 2000 Mu (Malvern, UK) laser particle size analyzer was used to examine the particle size distributions of CCPs.

A Synchronous Thermal Analyzer (STA 449 F5 Jupiter, Selb, Germany) produced by NETZSCH was used to measure the thermal decomposition process of powders consisting of CL-20/AP mixtures. Ar was used as a protective gas in the experiment and the flow rate was 100 mL·min^{-1}. The temperature ranged from room temperature to 600 °C, with a heating rate of 5 K·min^{-1}. Approximately 1 mg of sample was loaded for each test.
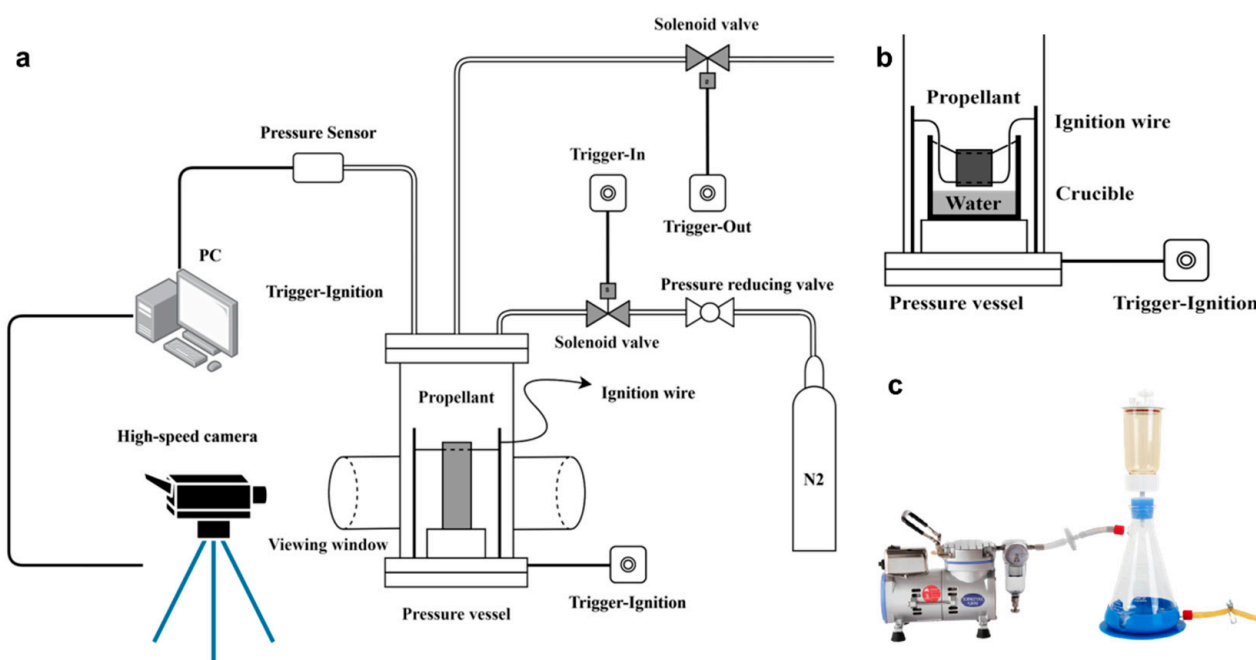
Figure 1. Schematic diagram of the experimental system: (**a**) Experimental system used for combustion surface agglomeration photography; (**b**) Combustion product collection device with cooling medium; (**c**) Vacuum filtration device.

3. Results and Discussion

3.1. Effect of CL-20 on AP Decomposition

The thermal decomposition characteristics of CL-20 on AP were obtained by thermogravimetric differential scanning calorimetry (TG-DSC) measurements with a thermal analysis system. The TG-DSC curves of the four different samples are shown in Figure 2. For pure AP, as shown in Figure 2a, the endothermic peak at 241.4 °C was the peak of the transition of the AP crystals from orthorhombic to cubic. When the temperature increased to 285.9 °C, the exothermic peak corresponded to the first low-temperature thermal decomposition of AP and the sample entered a slow weight-loss process with a weight loss of ~26.07%. When the temperature increased to 389.9 °C, the endothermic peak corresponded to the second high-temperature thermal decomposition of AP. During this process, the sample enters a rapid weight loss process, with a weight loss of ~99.52%.

The decomposition mechanism of AP is split into two stages [25]. The first stage of the decomposition is carried out on the local position of the crystal surface. The AP crystal surface contains defects, cracks, and other force-field non-saturation points, which are potential activation centers of the solid decomposition of AP. However, because the first stage of the decomposition is the formation of NH_3 and $HClO_4$ by proton transfer dissociation of AP, the low-temperature decomposition reaction involves gaseous NH_3 and gaseous $HClO_4$ adsorbed on the AP crystal surface. As the adsorbed NH_3 cannot be completely oxidized by the decomposition products of $HClO_4$ at low temperature, NH_3 continues to cover the crystal surface during the decomposition process. If it covers all activation centers on the surface, the decomposition process will stop. With the increase in the temperature, the potential reaction center is reactivated due to the desorption of NH_3 or the reaction takes place throughout the condensed phase after partial liquefaction of AP. The reaction does not include a "local chemistry" process, becomes more violent, and the mass of the solid phase decreases rapidly. This is the second stage of the AP decomposition.
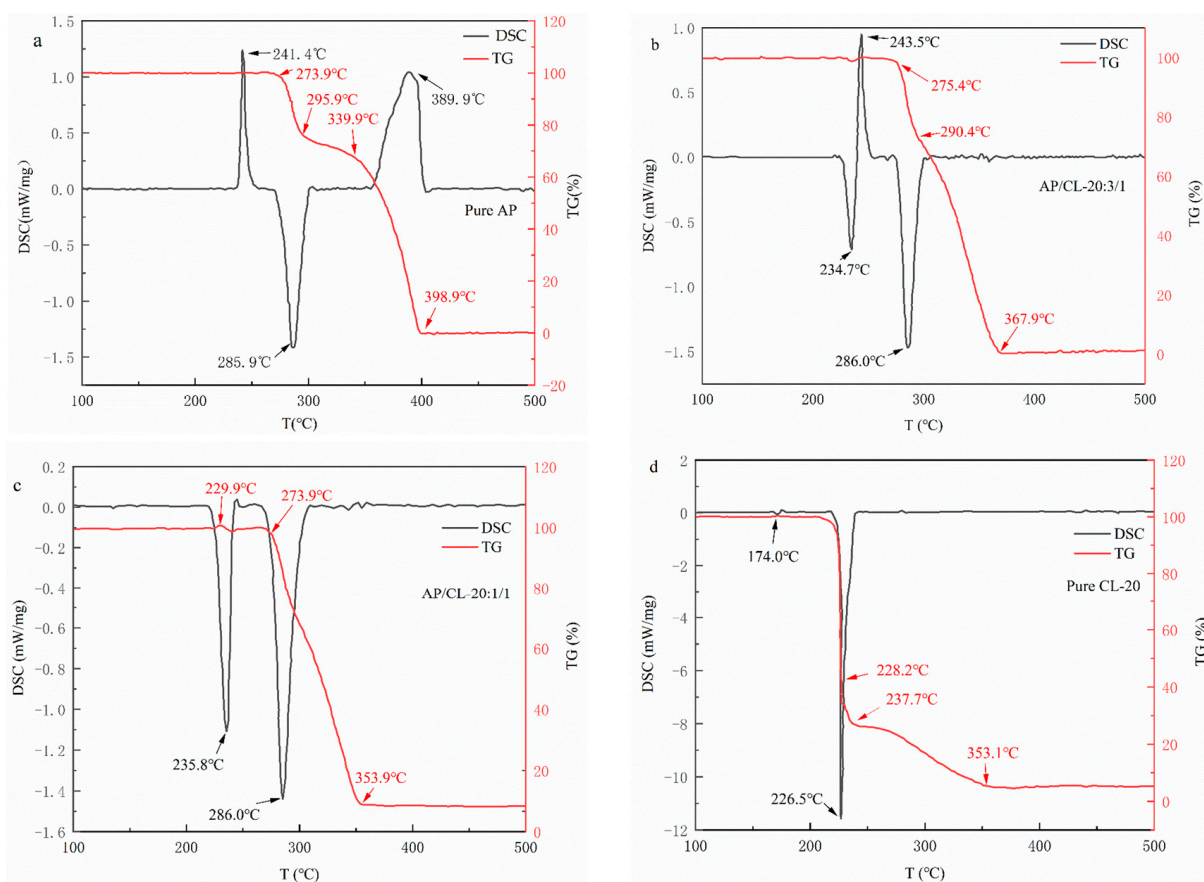
Figure 2. TG-DSC curves for four different samples: (**a**) Pure AP; (**b**) 75% AP/25% CL-20; (**c**) 50% AP/50% CL-20; and (**d**) Pure CL-20. Ar was used as protective gas and the flow rate was 100 mL·min^{-1}. The temperature ranges from room temperature to 600 °C, with a heating rate of 5 °C·min^{-1}. Approximately 1 mg of the sample was loaded for each test.

Figure 2b shows the TG-DSC curves of 25% CL-20 and 75% AP. As the proportion of CL-20 in the sample was relatively small, the decomposition of CL-20 did not cause significant changes in the mass of the solid phase. When the temperature increased to 243.5 °C, the endothermic peak represents the peak of the transition of the AP crystal from the orthorhombic to the cubic crystal system. The temperature then continued to increase to 286.0 °C. The exothermic peak corresponds to the high-temperature decomposition process of AP. At this time, the sample entered the rapid weight loss process with a weight loss of ~99.2%. Compared with pure AP, CL-20 can lower the reaction temperature of AP decomposition at high temperature, indicating that CL-20 promotes the decomposition of AP.

Figure 2c displays the half CL-20 and half AP of the TG-DSC curves. The exothermic peak at 235.8 °C corresponds to the thermal decomposition of CL-20; the temperature increased to 243.5 °C, the curve slightly protrudes upward, and the corresponding endothermic peak is the peak of the transition of the AP crystal from the orthorhombic to cubic crystal system. Subsequently, the temperature continued to increase to 286.0 °C. The exothermic peak corresponds to the high-temperature AP decomposition process. At this time, the sample entered a rapid weight loss process with a weight loss of ~91.4%. Based on the comparison of the three samples of pure AP, 50% AP, and 75% AP, the addition of CL-20 significantly reduced the energy required for the transition of AP crystals from the orthorhombic to cubic crystal system, and increased the energy released during the high-temperature decomposition of AP.

Figure 2d shows the DSC-TG curve of pure CL-20. The exothermic peak at 226.5 °C corresponds to the thermal decomposition of CL-20, during which the mass of the solid phase of the sample rapidly decreased. The weight loss of this process was ~97.2%. Based on

the comparison of the two samples of 50% AP and 0% AP, AP increased the decomposition temperature of CL-20. The exothermic heat corresponding to the decomposition peak of CL-20 shown in Figure 2b,c is reduced by more than ten times when compared to pure AP and pure CL-20, and the solid phase weight loss is not apparent, indicating that only a small portion of CL-20 is decomposed. It has been shown that the decomposition peak of the second stage of AP is endothermic peak or exothermic peak, which depends on the competitive trend between AP dissociation and sublimation [26]. It is hypothesized that CL-20 and AP interact, resulting in only a small amount of CL-20 being decomposed at the original exothermic peak position. The dissociation of the remaining CL-20 at the second endothermic peak of AP changes the competitive relationship between AP dissociation and sublimation, and the second endothermic peak of AP vanishes.

3.2. Agglomeration Characteristics

A high-speed camera was used to observe the aluminum agglomeration phenomenon near the three propellants' burning surface. Figure 3 shows the agglomeration of aluminum in the three samples. Based on the high-speed video, aluminum agglomerates were formed on the propellant surface and gradually separated from the combustion surface. The three stages of the aluminum agglomeration are accumulation, aggregation, and agglomeration. During the combustion process, the local temperature of the burning surface reaches the melting point of Al_2O_3 (~2300 K). The aluminum particles in the propellant gradually detach from the propellant surface and congregate at the burning surface, which is covered with Al_2O_3 as shown in Figure 3a(1). Due to the air flow near the burning surface, adjacent accumulations will approach each other until they fuse together, as shown in Figure 3a(2–4). When the Al_2O_3 shell on the surface is thermally broken, the aluminum particles inside begin to agglomerate. The shape also changes from coral shape to regular spherical shape, and agglomerates are pushed away from the combustion surface by the gas as shown in Figure 3a(5–9). The Al_2O_3 shell moves and reacts in a closed container and finally forms agglomerates after cooling. Some agglomerates collide with adjacent agglomerates after detaching from the combustion surface and finally fuse into new agglomerates. From another perspective, it has been proven that there are certain errors in the characterization of the agglomerates near the burning surface through the physical and chemical characteristics of agglomerates in CCPs.

Figure 3b shows the process from the formation of aluminum agglomerates on the burning surface to their detachment from the burning surface related to propellant C2 at 1 MPa. Compared with Figure 3a, the particle size of the agglomerates created by the combustion of the C2 propellant was considerably smaller than that of the C1 propellant. The high-speed video of the combustion process of C1 and C2 propellants shows that the agglomerates stayed on the combustion surface for a long time during the combustion process of the C1 propellant before their morphologies changed from coral to spherical shapes and separated from the combustion surface. In this process, adjacent agglomerates were likely to fuse to form larger agglomerates. In contrast, the agglomerates only stayed on the combustion surface for a short time during the combustion of the C2 propellant before they were blown away. The probability of volume growth of the agglomerates after merging with other agglomerates, and the overall particle size of the agglomerates, significantly reduced. It can be speculated that this process is related to the particle size of AP. AP with smaller particle size decomposes much faster, in a manner where the agglomerates can separate from the combustion surface at a faster rate. As shown in Table 1, the particle size of AP used in the C1 propellant was 116 μm, whereas that used in the C2 propellant was 69 μm. It can be speculated that the use of AP with a smaller particle size weakens the agglomeration phenomenon in the combustion process and reduces the agglomerate with a large particle size generated by combustion. This agrees with the results of previous studies on the effect of the AP particle size on the agglomeration of the burning surface and the characteristics of the CCPs of CL-20 propellant. Figure 3c shows the process from the formation of aluminum agglomerates on the combustion surface to

the separation from the combustion surface of propellant C3, photographed at 1 MPa, and the fusion of other agglomerates nearby. Compared with Figure 3b, the particle size of the agglomerates produced by the combustion of the C3 propellant was significantly larger than that of the C2 propellant. Aluminum agglomerates first formed, accumulated, and then detached from the combustion surface, as shown in Figure 3b(1–3). After leaving the burning surface, some of the agglomerates collided with nearby agglomerates and fused to form new agglomerates with larger particle sizes, as shown in Figure 3c(4–9).
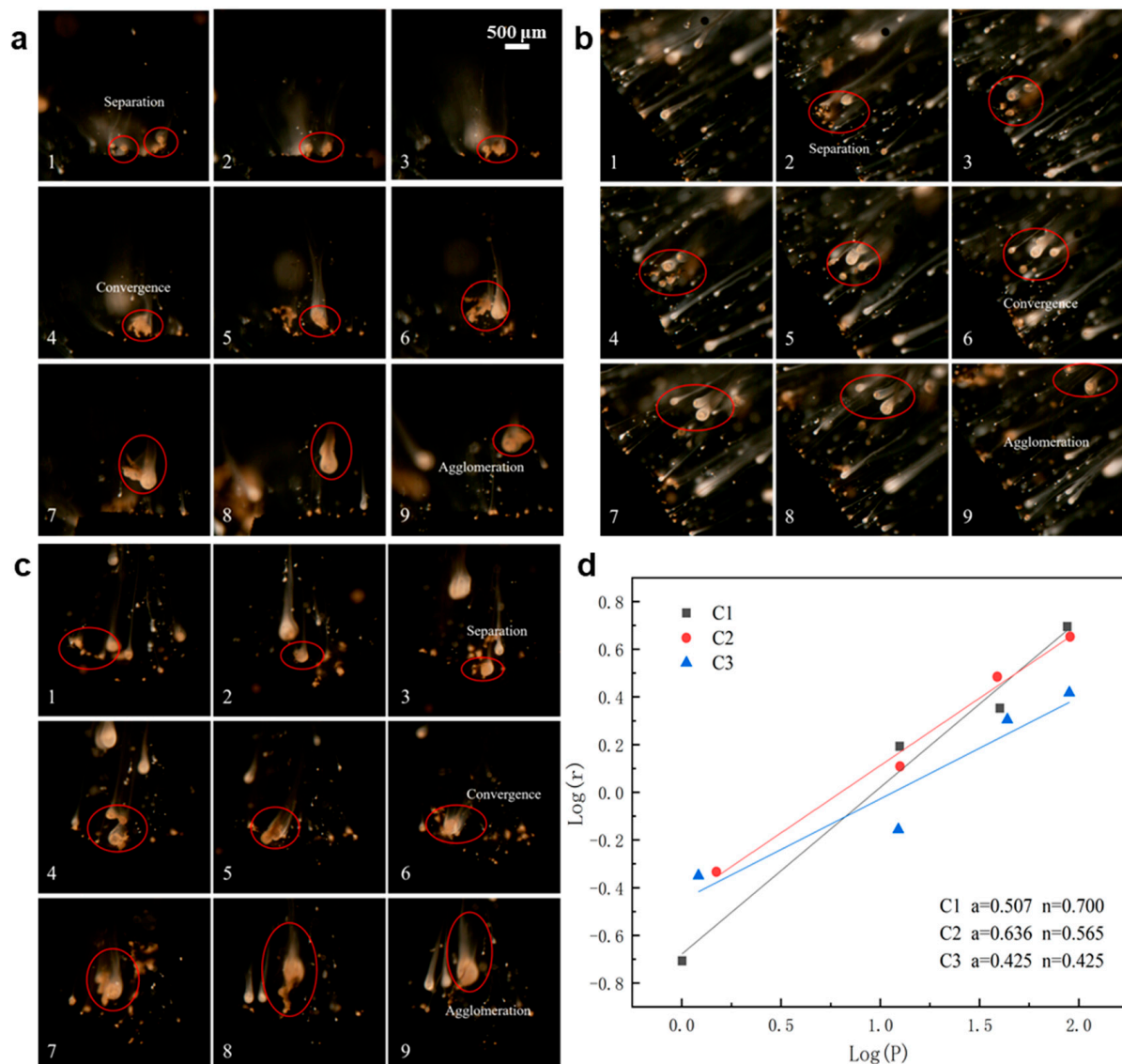

Figure 3. Surface agglomerates of three different samples: (**a**) C1 propellant, (**b**) C2 propellant, (**c**) C3 propellant, and (**d**) Processing and fitting of the combustion data of propellant samples: The fitted line connected by black and gray (squares) are C1 propellants, while red (circles) and blue (triangles) represent C2 and C3 propellants, respectively. The fitting equation is as follows: $\ln r = n \ln P + \ln a$, where r is the burning rate (mm·s^{-1}), a is the burning rate coefficient, P is the combustor pressure (MPa), and n is the pressure exponent.

The analysis shows that agglomeration can be attenuated by using AP with a smaller particle size in the propellant during combustion, which reduces the large particle sizes of agglomerates caused by combustion. At low combustion chamber pressure, the agglomerates of AP with smaller particle sizes and the propellant with higher CL-20 content will be blown away from the combustion surface, after being on the surface for a short time. In this

process, the probability of agglomerate volume growth after merging with other agglomerates greatly reduces, and thus, the overall particle sizes of the agglomerates decrease.

Figure 3d illustrates the reduction in the propellant's pressure exponent, that is, the sensitivity to pressure changes, upon addition of AP particles with smaller particle sizes leading to a more stable combustion process. The addition of CL-20 improved the energy characteristics and burning rate and increased the pressure exponent of the propellant. Based on the heat transfer model of the CL-20 combustion wave [27], CL-20 is an ammonium nitrate explosive, which contains large amounts of NO and NO_2 in the gaseous phase reaction region and the reaction between NO and NO_2 is generally a three-molecule reaction. These responses are highly sensitive to pressure. The burning rates of C2 and C3 are similar, and the agglomeration is much smaller. Based on the addition of CL-20 to burning surface particles, ignition becomes easier and the number of ignited particles is larger, indicating that the high-energy nature of CL-20 releases a large amount of heat, which strengthens the ignition of aluminum particles and inhibits the agglomeration process.

3.3. CCP Properties

The CCP collection test system was used to quench the CCPs of three propellants under different pressures. Subsequently, the particle size distributions were analyzed. The physicochemical indices were tested using SEM, XRD, and laser particle size tests. The CCPs of aluminum-based composite propellants generally include agglomerates and alumina soot particles. Figure 4a–d show the CCPs morphology. In the combustion products, the agglomerates mostly had a relatively regular spherical shape with a small part broken or agglomerated. The particle size of the agglomerates generally reached several hundreds of microns. Figure 4d shows that several spherical particles formed agglomerates with large particle sizes after melting. Figure 4b shows that the surface of the agglomerate is not smooth. A large number of small-sized particles are attached to the agglomerated particle surface, most of which are spherical or ellipsoidal and have a particle size of ~1 μm. It can be speculated that smoke oxide particles or aluminum vapor condense on the surface because CCPs are generated by the combustion of propellant in a closed burner, causing a huge number of tiny particles to adhere to the surface. Moreover, the hollow structure can be observed in the partially broken agglomerate particles. In the combustion process, the aluminum particles of the propellant are covered with alumina shells with higher melting points. Internal aluminum particles are constantly burned, consumed, melted, and evaporated, whereas the external aluminum shell gradually cools. After the combustion, the aluminum inside the agglomerate is exhausted and only the external aluminum shell remains.

Figure 4e shows irregular coral-like shapes with particle sizes that generally reach up to several hundreds of microns. Compared with Figure 4e, Figure 4f shows uneven CCPs, but the surface of the agglomerates is relatively smooth, most of which are spherical or ellipsoidal. Particles are generally tens of microns in size. It has been hypothesized that an AP-fuel micro-element flame easily forms when the AP particle size increases and the flame is closer to the burning surface, which is conducive to the ignition of aluminum powder. On the contrary, larger fine AP particles can also encapsulate the aluminum powder, reducing the volume of the effective "pocket" [28]. Both are beneficial to the reduction in the particle size of aluminum agglomerates. Compared with Figure 4f, Figure 4g shows that the surface of the agglomerates is relatively smooth; most of them are spherical and a few hundred microns in size. It can be speculated that increasing the CL-20 content improves the combustion efficiency of Al and reduces the agglomerate particle size. Figure 4h–k shows that the particle sizes of agglomerates decrease with the increase in the pressure, which is presumed to be caused by the more sufficient reaction at higher pressure.
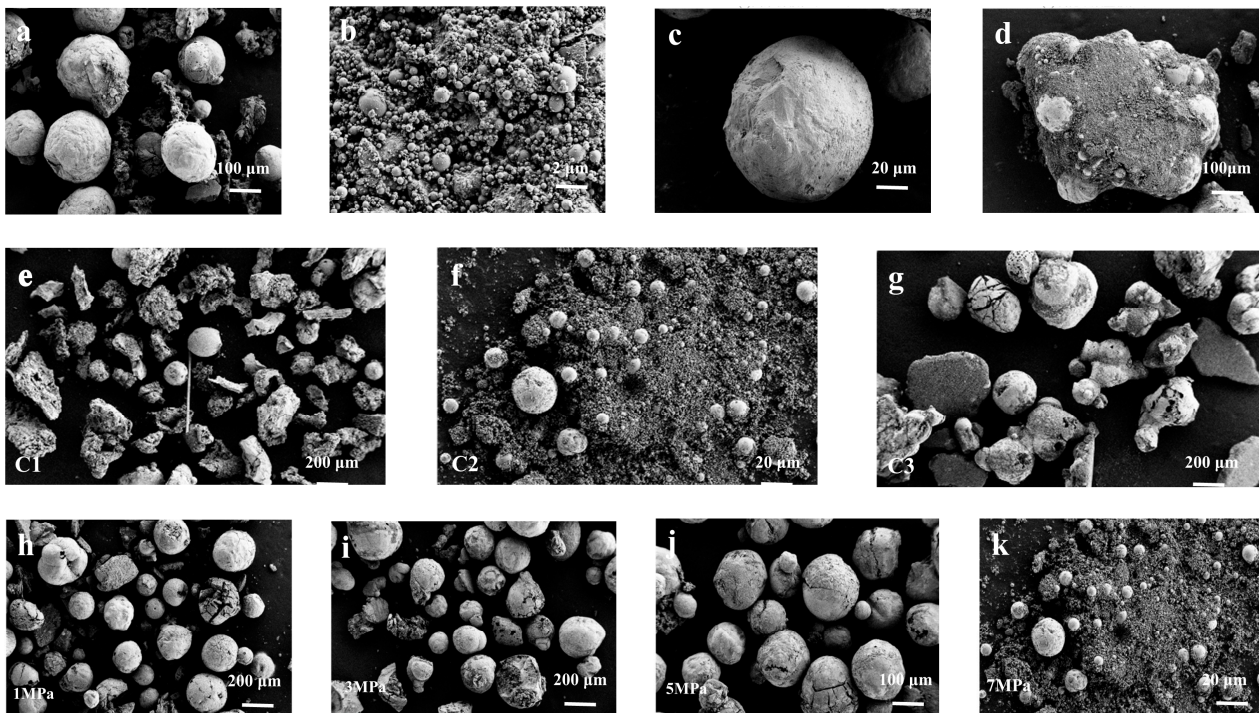
Figure 4. SEM images of the CCPs of three propellants: (**a–d**) Typical morphology of CCPs for C1 propellent; (**e–g**) C1, C2, C3 propellant microstructure of CCPs; (**h–k**) Four different pressure C2 propellant microstructures of CCPs.

The agglomeration degree of aluminum particles in combustion products was characterized using the volume mean diameter D [4,3] of CCPs. Although the particle size of CCPs collected in the cooling medium was smaller than that of the agglomerate at the combustion surface after a period of combustion in the combustion chamber, the particle size distribution of CCPs can still be used to determine the characteristics of the agglomerate at the combustion surface of the propellant. Table 2 shows the D [4,3] values, peak particle size, and corresponding volume fraction of CCPs for the three propellants at different pressures. The D [4,3] value of propellant C1 is significantly larger than that of C2 and C3, demonstrating the presence of more large-sized agglomerate particles in the CCPs of the C1 propellant. At lower pressure, the D [4,3] value of C3 is significantly larger than that of C2, whereas the D [4,3] value of C3 is slightly smaller than that of C2 at high pressure, but the peak particle size and corresponding volume fraction of C3 are larger than those of C2.

Table 2. CCPs peak particle size and D [4,3] at different pressures.

Pressure/MPa	Propellant Number	C1	C2	C3
1	D [4,3] (μm)	305.892	273.98	428.061
	Peak particle size (μm)	447.74	282.5	447.74
	volume fraction (%)	6.39	9.92	11.19
3	D [4,3] (μm)	215.896	74.992	192.06
	Peak particle size (μm)	251.78	100.23	251.78
	volume fraction (%)	7.64	5.65	7.44
5	D [4,3] (μm)	246.683	91.938	64.744
	Peak particle size (μm)	282.5	79.62	141.58
	volume fraction (%)	5.7	3.94	3.73
7	D [4,3] (μm)	250.611	48.741	46.565
	Peak particle size (μm)	355.65	50.24	100.23
	volume fraction (%)	5.74	1.93	3.09

The CCP particle size distribution of the three propellants at 7 MPa is shown in Figure 5a. Based on the comparison of C1 and C2 propellants, the peak particle size and corresponding volume fraction of CCPs of the C2 propellant are significantly lower than those of the C1 propellant. As shown in Table 1, the AP particle size used in C1 propellant is 116 μm and that of C2 is 69 μm. It can be speculated that the use of AP with a smaller particle size in the propellant reduced the agglomeration in the combustion process. In addition, the particle size and corresponding volume fraction of the large particle size of combustion products can be reduced. Based on the comparison of C2 and C3 propellants, the peak particle size and corresponding volume fraction of CCPs in the C2 propellant were significantly lower than those in the C3 propellant and showed bimodal characteristics. As shown in Table 2, the particle size D [4,3] of CCPs in the C2 propellant was smaller than that in C3 at 1–3 MPa and larger than that in C3 at 5–7 MPa. The mass fraction of CL-20 and AP in C2 and C3 were 42% and 12%, respectively, and 20% and 34%. According to previous studies, the particle size of aluminum agglomerates decreases with the increase in AP relative content [29], so it can be speculated that adding a certain proportion of CL-20 to the propellant increases the energy and reduces the particle size of the agglomerates at low pressure. The advantage increases with increasing CL-20 proportion, while it is the opposite at high pressure. It can be speculated that this result is related to the large increase in the propellant pressure exponent after the addition of CL-20.

Figure 5b shows the diffraction patterns of the CCPs of the propellants at 7 MPa. Compared with the standard card, the CCPs of the three propellant samples mainly contain Al_2O_3 and Al. Compared with C2, the diffraction peak of Al in the CCPs of C2 propellant was significantly lower than that of C1 and the diffraction peak of Al_2O_3 was significantly higher than that of C1. As the AP particle size of C1 is 116 μm and that of C2 is 69 μm, it can be speculated that AP with a smaller particle size is more conducive to propellant combustion such that the energy in the propellant can be released more completely. Compared with C3, the diffraction peak of Al_2O_3 in the CCPs of the C2 propellant is slightly higher than that of C3. This suggests that within a certain range, the higher the mass fraction of CL-20 in the propellant is, the more complete is the combustion of the propellant.
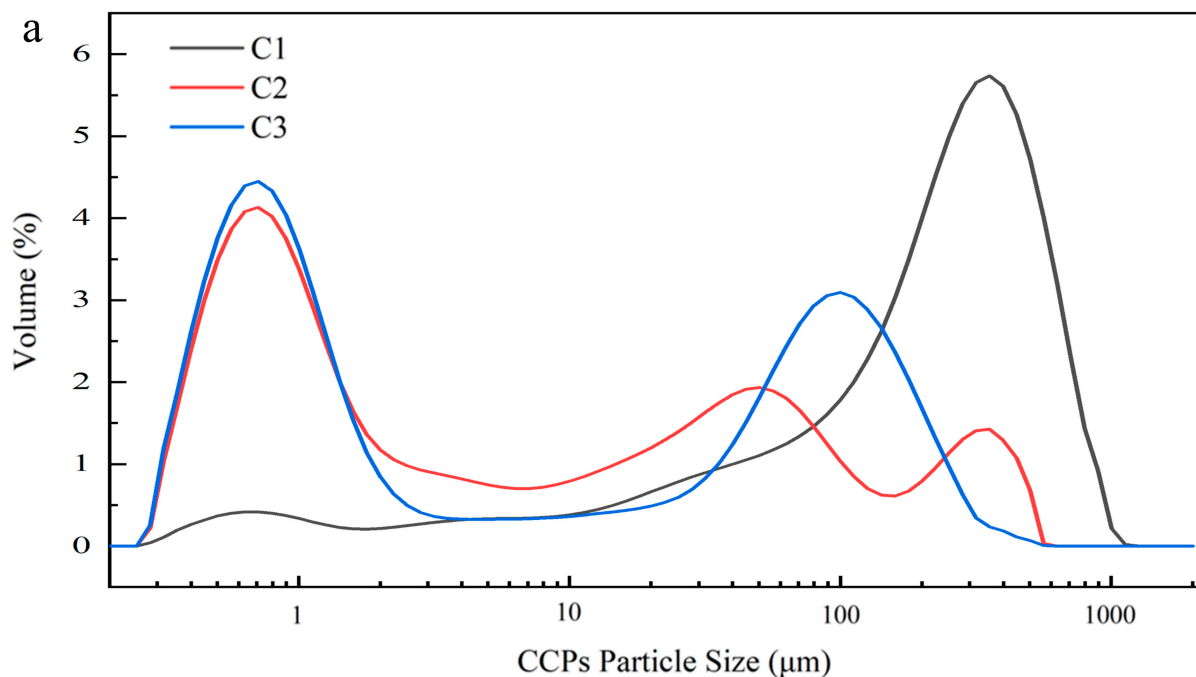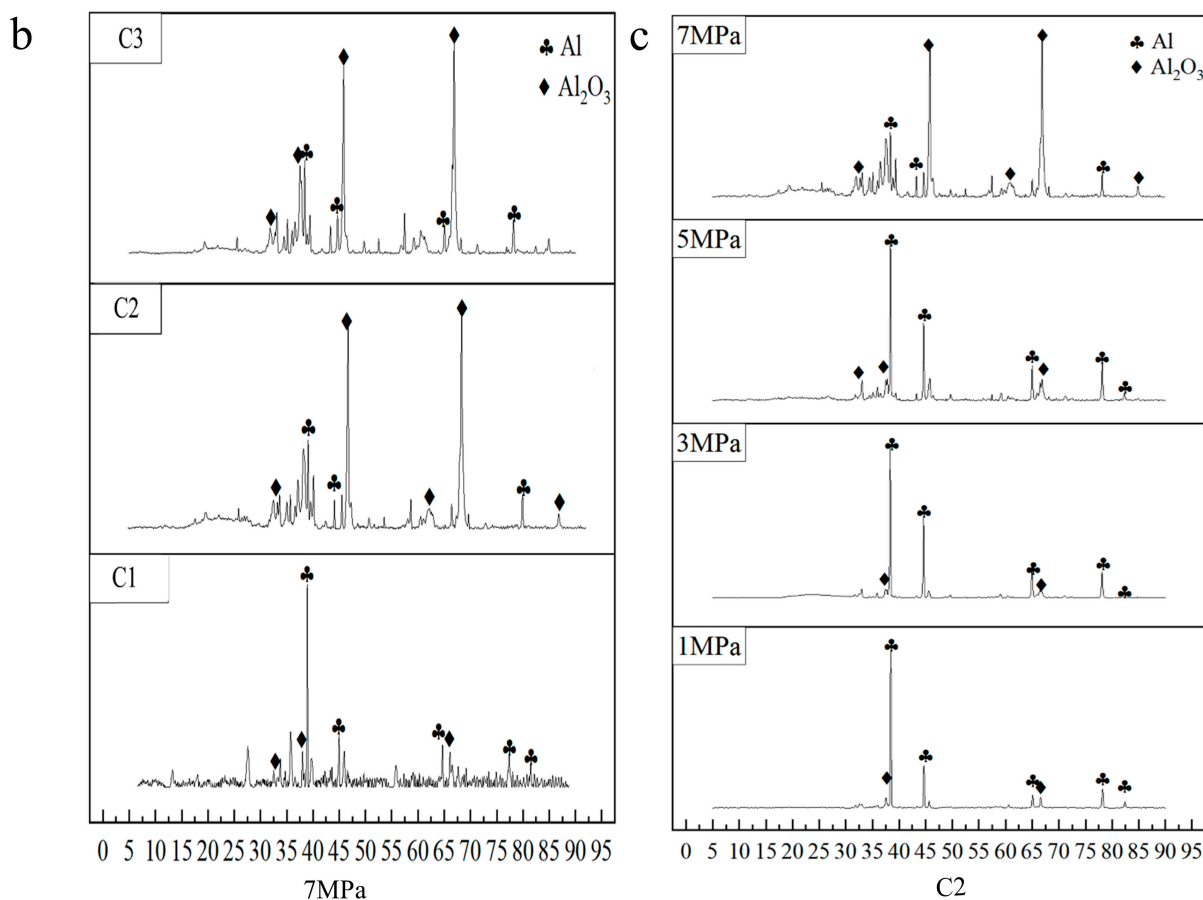

Figure 5. *Cont.*

Figure 5. XRD pattern of CCPs: (**a**) CCP particle size distribution of three propellants at 7 MPa; (**b**) Comparison of the combustion efficiency of three propellants at 7 MPa; (**c**) XRD pattern of the C2 propellant.

4. Conclusions

In this study, the effects of AP and CL-20 on the thermal decomposition, combustion, and agglomeration characteristics of aluminum-based composite propellants were explored from multiple dimensions including the energy characteristics and combustion products.

Based on the burning rate test, a smaller AP particle size leads to a lower pressure exponent of the propellant; that is, a reduction in the sensitivity to pressure changes, and thus, a more stable combustion process. The addition of CL-20 to the propellant improves its energy characteristics and combustion rate, but also increases its pressure exponent. By photographing the process of aluminum agglomerates forming on the propellant surface and gradually breaking away from the burning surface, the pathway of aluminum particles from aggregation to agglomeration on the burning surface was analyzed, and the effects of different AP particle sizes and CL-20 ratios on aluminum agglomeration were determined. In addition, the physical and chemical indexes of CCPs were analyzed using SEM, XRD, and laser particle size tests. AP with a small particle size improves the reaction of Al particles in the propellant and reduces the occurrence of agglomeration. Generally, CL-20 in the propellant increases the energy and reduces the particle size of agglomerates. A higher proportion of CL-20 is beneficial to the full reaction of Al particles.

References

1. Liu, T.K.; Perng, H.C.; Luh, S.P.; Liu, F. Aluminum Agglomeration in Ammonium Perchlorate/Cyclotrimethylene Trinitramine/Aluminum/Hydroxy-Terminated Polybutadiene Propellant Combustion. *J. Propul. Power* **1992**, *8*, 1177–1184. [CrossRef]
2. Takahashi, K.; Oide, S.; Kuwahara, T. Agglomeration Characteristics of Aluminum Particles in AP/AN Composite Propellants. *Propellants Explos. Pyrotech.* **2013**, *38*, 555–562. [CrossRef]
3. Liu, L.; Ao, W.; Wen, Z.; Wang, Y.; Long, Y.; Liu, P.; He, G.; Li, L.K.B. Modifying the Ignition, Combustion and Agglomeration Characteristics of Composite Propellants via Al-Mg Alloy Additives. *Combust. Flame* **2022**, *238*, 111926. [CrossRef]
4. Ao, W.; Fan, Z.; Liu, L.; An, Y.; Ren, J.; Zhao, M.; Liu, P.; Li, L.K.B. Agglomeration and Combustion Characteristics of Solid Composite Propellants Containing Aluminum-Based Alloys. *Combust. Flame* **2020**, *220*, 288–297. [CrossRef]
5. Anand, K.V.; Roy, A.; Mulla, I.; Balbudhe, K.; Jayaraman, K.; Chakravarthy, S.R. Experimental Data and Model Predictions of Aluminium Agglomeration in Ammonium Perchlorate-Based Composite Propellants Including Plateau-Burning Formulations. *Proc. Combust. Inst.* **2013**, *34*, 2139–2146. [CrossRef]
6. Babuk, V.A.; Vasilyev, V.A.; Malakhov, M.S. Condensed Combustion Products at the Burning Surface of Aluminized Solid Propellant. *J. Propul. Power* **1999**, *15*, 783–793. [CrossRef]
7. Ao, W.; Wen, Z.; Liu, L.; Liu, P.; Gan, Y.; Wang, L.; Li, L.K.B. Controlling the Combustion and Agglomeration Characteristics of a Solid Composite Propellant via a DC Electric Field. *Aerosp. Sci. Technol.* **2022**, *128*, 107766. [CrossRef]
8. Glotov, O.G. Condensed Combustion Products of Aluminized Propellants. IV. Effect of the Nature of Nitramines on Aluminum Agglomeration and Combustion Efficiency. Combust. Explos. *Shock Waves* **2006**, *42*, 436–449. [CrossRef]
9. Jacob, R.J.; Jian, G.; Guerieri, P.M.; Zachariah, M.R. Energy Release Pathways in Nanothermites Follow Through the Condensed State. *Combust. Flame* **2015**, *162*, 258–264. [CrossRef]
10. Babuk, V.A.; Vassiliev, V.A.; Sviridov, V.V. Propellant Formulation Factors and Metal Agglomeration in Combustion of Aluminized Solid Rocket Propellant. *Combust. Sci. Technol.* **2001**, *163*, 261–289. [CrossRef]
11. Ao, W.; Wen, Z.; Liu, L.; Wang, Y.; Zhang, Y.; Liu, P.; Qin, Z.; Li, L.K.B. Combustion and Agglomeration Characteristics of Aluminized Propellants Containing Al/CuO/PVDF Metastable Intermolecular Composites: A Highly Adjustable Functional Catalyst. *Combust. Flame* **2022**, *241*, 112110. [CrossRef]
12. Liu, L.; Ao, W.; Wen, Z.; Zhang, Y.; Lv, X.; Qin, Z.; Liu, P. Combustion Promotion and Agglomeration Reduction of the Composite Propellant Using Graphene. Aerosp. *Sci. Technol.* **2021**, *118*, 106988. [CrossRef]
13. Gao, Y.; Ao, W.; Li, L.K.B.; Zhou, S.; He, W.; Liu, P.; Yan, Q.-L. Catalyzed Combustion of a Nanofluid Fuel Droplet Containing Polydopamine-Coated Metastable Intermixed Composite n-Al/CuO. *Aerosp. Sci. Technol.* **2021**, *118*, 107005. [CrossRef]
14. Ao, W.; Liu, P.; Liu, H.; Wu, S.; Tao, B.; Huang, X.; Li, L.K.B. Tuning the Agglomeration and Combustion Characteristics of Aluminized Propellants via a New Functionalized Fluoropolymer. *Chem. Eng. J.* **2020**, *382*, 122987. [CrossRef]
15. Ao, W.; Liu, P.; Lv, X.; Yang, W. Review of Aluminum Agglomeration During the Combustion of Solid Propellants. *J. Astronaut.* **2016**, *37*, 371–380. [CrossRef]
16. Liu, H.; Ao, W.; Hu, Q.; Liu, P.; Hu, S.; Liu, L.; Wang, Y. Effect of RDX Content on the Agglomeration, Combustion and Condensed Combustion Products of an Aluminized HTPB Propellant. *Acta Astronaut.* **2020**, *170*, 198–205. [CrossRef]
17. Ding, L.; Zhao, F.Q.; Li, S.W.; Xu, H.X.; Yi, J.H. Combustion Property of NEPE Propellant with CL-20. *Chin. J. Energ. Mater.* **2007**, *19*, 68–77. [CrossRef]
18. Zhou, S.; Zhou, X.; Tang, G.; Guo, X.; Pang, A. Differences of Thermal Decomposition Behaviors and Combustion Properties Between CL-20-based Propellants and HMX-Based Solid Propellants. *J. Therm. Anal. Calorim.* **2020**, *140*, 2529–2540. [CrossRef]
19. Zhou, S.; Wu, F.; Tang, G.; Wang, Y.; Pang, A.; Song, H.; Wang, Y. Influence of CL-20 Content and Its Particle Size Gradation on Combustion Performance of NEPE Propellants. *Chin. J. Explos. Propellants* **2020**, *43*, 195–202. [CrossRef]
20. Ding, L.; Zhao, F.Q.; Pan, Q.; Xu, H.X. Research on the Thermal Decomposition Behavior of NEPE Propellant Containing CL-20. *J. Anal. Appl. Pyrol.* **2016**, *121*, 121–127. [CrossRef]
21. Wu, H.; Chen, L.; Dong, X.; Ao, W.; Liu, L. Effects of Particle Size of Al and AP on Agglomeration and Properties of Condensed Combustion Products of CL-20 Propellant. *Chin. J. Explos. Propellants* **2021**, *44*, 367–371. [CrossRef]
22. Song, Z.; Yan, Q.; Li, X.; Liu, P.; Zhao, Y. Effects of CL-20 on the Condensed Combustion Products of Al/HMX-XLDB Propellants. *J. Combust. Sci. Technol.* **2013**, *19*, 241–247.

23. Zhou, X.; Tang, G.; Pang, A.; Fang, W.U.; Song, H.; Haiyuan, X.U.; Wang, Y.; Xingxing, X.U.; Zhou, S. Effect of Content of Solid Components on Combustion Performance of GAP/CL-20 Propellant. *J. Solid Rocket Technol.* **2017**, *40*, 720–724. [CrossRef]

24. Zhao, Y.; Tian, D.; Jiang, Y. Combustion Simulation of Aluminum-Containing Composite Propellant. *J. Aerosp. Power.* **1987**, *2*, 147–152+188–189. [CrossRef]

25. Boldyrev, V.V. Thermal decomposition of ammonium perchlorate. *Thermochim. Acta* **2006**, *443*, 1–36. [CrossRef]

26. Shen, X.; Wang, D.; Cheng, L.; Ji, Y. Effect of Fresh Catalysts on Thermal Decomposition of AP. In Proceedings of the Third Aero Power Joint Conference, Big Sky, MT, USA, 9 July 2018; pp. 32–40.

27. Sinditskii, V.P.; Chernyi, A.N.; Egorshev, V.Y.; Dashko, D.V.; Goncharov, T.K.; Shishov, N.I. Combustion of CL-20 Cocrystals. *Combust. Flame* **2019**, *207*, 51–62. [CrossRef]

28. Ao, W.; Liu, X.; Rezaiguia, H.; Liu, H.; Wang, Z.X.; Liu, P.J. Aluminum Agglomeration Involving the Second Mergence of Agglomerates on the Solid Propellants Burning Surface: Experiments and Modeling. *ACTA Astronaut.* **2017**, *136*, 219–229. [CrossRef]

29. Sambamurthi, J.K.; Price, E.W.; Sigmant, R.K. Aluminum Agglomeration in Solid-Propellant Combustion. *AIAA J.* **1984**, *22*, 1132–1138. [CrossRef]